Optical study of the pseudogap in thickness and orientation controlled artificial opals

J.F. Galisteo-López, E. Palacios-Lidón, E. Castillo-Martínez, C. López[a)]

Instituto de Ciencia de Materiales de Madrid, Cantoblanco 28049-Madrid, Spain

Artificial opals consisting of polystyrene spheres ordered into a *fcc* lattice are grown with control over orientation and thickness. A thorough study of the formation of the pseudogap in these structures is carried out by means of reflectivity and transmission spectra. Special attention is paid to discriminate those features inherent to the photonic crystal, and those to the substrate on which the crystal is grown. Further, a characterization of the photonic band structure in the hexagonal facet of the Brillouin zone is made using angle resolved reflectivity measurements.

[a)] Electronic mail: cefe@icmm.csic.es

I. INTRODUCTION

Due to the ability of monodisperse submicrometer spherical polymer or glass particles to self assemble into *fcc* ordered three dimensional (3D) structures, they have been proposed as a playground to test the optical properties of a novel type of materials known as photonic crystals [1,2]. These materials consist of a composite dielectric with a periodically varying refractive index. Light propagating through a given direction inside the crystal will be Bragg diffracted, its dispersion relation branching into a series of allowed and forbidden bands, the latter known as stop bands. Under specific conditions regarding the refractive index contrast and topology of the structure [3,4], stop bands along every direction of propagation may share a common interval of frequencies in which electromagnetic modes will be forbidden: a photonic band gap. While the existence of stop bands implies forbidden frequency channels for the propagation of light along certain directions, it is in the presence of a photonic band gap that spectacular phenomena have been predicted [5, 6]. For frequencies contained in this interval, the density of photonic states becomes zero and the radiation dynamics of active centers embedded in the crystal may be altered, allowing the complete inhibition of spontaneous emission of excited atoms or molecules [1]. Although a great deal of attention has been paid to phenomena having its origin in the existence of a photonic band gap, there is a growing interest on allowed bands where the propagation of light may exhibit anomalous refraction. Photonic crystals may then behave as superprisms [7] or negative refractive index materials without absorption [8].

The ability to control the flow of light in the above mentioned manners has gained for photonic crystals an additional interest in terms of industrial applications. Proposals have been made to employ these structures as low-threshold lasers [9], efficient collimators [10] or all-optical microchips [11] to name a few. Whether the use

of the crystal is based on the existence of a photonic band gap, or the propagation along allowed bands, predictions are made in most cases based on the photonic band structure of the system, which serves as a powerful tool for describing light propagation in infinite structures [12]. Since any attempt to implement photonic structures into industrial devices will certainly require the use of finite structures, the question arises on how does the finite crystal compare to the infinite system described by photonic bands, in terms of its optical properties. Finite size effects [13] as well as disorder [14, 15, 16, 17, 18, 19, 20], always present in real crystals, are likely to modify the optical behavior of the finite real system in comparison with the infinite ideal one. Further, concepts such as density of states, fundamental for a description of the dynamics of excited atoms inside a photonic crystal, cannot be directly translated into finite structures [21]. It seems then, that a proper knowledge of the optical properties of finite photonic crystals is mandatory prior to consideration for any application.

In this work we have studied the formation of the pseudogap associated with the (111) family of planes in opal based photonic crystals, as a function of the thickness in the direction perpendicular to the planes, by means of reflection and transmission measurements. In doing so we have discriminated between those features of experimental spectra dependant on the substrate on which the sample is grown, and those intrinsic to the interaction between electromagnetic radiation and the crystal. The effect of disorder on this process is also taken into account. Once the threshold for an infinite structure behavior is determined, an experimental study of the band-structure is performed by means of angle resolved reflectivity measurements.

II. PREPARATION AND STRUCTURAL CHARACTERIZATION OF SAMPLES

The samples used in this work are artificial opals consisting of polystyrene spheres ordered into a fcc lattice with the (111) family of planes parallel to the sample surface. Sample growth was carried out by the vertical deposition method [22]. Polystyrene spheres were synthesized by free emulsion polymerization [23] with a polydispersity <4%. Clean microslides were placed vertically in a vial containing an aqueous solution of polystyrene colloids, with a concentration ranging from 0.1 to 0.2%vol. The vial was then introduced in an oven where the temperature was controlled with a precision of 1ºC. The oven temperature was set to 45ºC and the sample was removed after 16 hours. Samples were also grown at higher and lower temperatures, although the quality was poorer, as indicated by optical spectroscopy. In these conditions, samples with typical lateral dimensions on the order of 1-2 cm^2 were grown. The number of layers present in samples grown in this way was controlled through colloid concentration. The main advantage of this procedure over other methods usually employed to grow artificial opals, such as sedimentation [24, 25, 26] or electrophoretic deposition [27], is that control is gained over the thickness and orientation of the sample, which is essential for the purpose of the work. Samples prepared by the latter methods usually yield specimens of uncontrollable thickness, presenting a polycrystalline nature [19, 28, 29], with domains randomly oriented both, with respect to their normal and in the plane.

To further study the influence of the substrate on the optical properties of the crystals, samples were grown on two different types of substrate: fused silica microslides, and silicon wafers. The diameter of the spheres used (500, 670 and 700nm) where chosen so that the spectral region of interest, that is, the position of the stop band

associated with the (111) family of planes, overlapped with the transparency region of the substrates.

Under the naked eye, our samples present bright iridescences when observed at certain angles, indicating the ordering of the spheres. Out of this angles, the samples are not fully transparent, indicating the presence of some disorder. In order to determine the orientation of samples grown by this method, we proceed as follows. When illuminated at normal incidence with monochromatic laser beams, our samples present a hexagonal diffraction pattern. This effect has its origin in light diffraction by the first layer of spheres and further projection on the sample-substrate interface [30, 31] and can be interpreted as the Fourier transform of the crystal surface, proving a valuable tool to control the orientation of the crystal. In the observed diffraction pattern, lines connecting the center to each of the six spots forming the hexagon can be associated to reciprocal lattice vectors of the 2D hexagonal array present at the surface. If the lines that bisect these vectors are drawn, a hexagon will appear, rotated 30^{o} with respect to the original one. This new hexagon is an image of the hexagonal facet of the first Brillouin zone of a fcc crystal structure centered at the *L* point. The observation of this pattern will allow us to properly orient the crystal when measuring angle resolved reflectivity.

To further confirm the above a closer examination was performed by means of scanning electron microscopy (SEM). Figure 1.a shows the crystal surface presenting the two dimensional (2D) hexagonal ordering of spheres, characteristic of (111) planes in fcc structures. The arrow indicates the direction in which the crystal growth takes place: along the vertical axis of the microslide and normal to the (111) family of planes. This shows how polystyrene spheres tend to assemble in rows parallel to the direction in which the meniscus is moving, that is, perpendicular to the meniscus itself. The inset

corresponds to the Fourier transform of the photograph, which coincides with the observed diffraction pattern (not shown). Furthermore, this pattern can be observed as the sample is translated in the plane perpendicular to the laser beam. This indicates that despite the fact that some cracks are found under SEM inspection of the samples (fig. 1b), all domains have the same orientation. Further, point defects and dislocations (fig. 1c) were to be found in most regions between the cracks.

It should be noted that the observation of this diffraction pattern represents a non destructive way of structural characterization of the samples, contrary to scanning electron microscopy where the optical properties of the sample are altered by the thin metal coating used to avoid the charging of the sample.

III. OPTICAL CHARACTERIZATION OF SAMPLES

Reflection and transmission spectroscopy are customary techniques which reveal stop bands as increased reflection or decreased transmission respectively, indicating the non-zero imaginary component of the wave-vector for those frequencies contained in the stop-band. In the presence of disorder, as is our case, experimental spectra obtained by transmission and reflection are affected differently. Reflection peaks tend to become less intense, asymmetric and may even become spectrally wider in the presence of a mosaic spread [18, 19, 32]. On the other hand, transmission spectra present an increased transmission in the stop band frequencies, as well as a background of decreased transmission for frequencies outside the stop band [13, 14, 16, 19]. The existence of this background makes the determination of quantities such as the full width at half maximum (FWHM), usually employed to determine the stop band width from experimental spectra [29, 33, 34], a non trivial task. For our samples, the above mentioned features are observed as can be seen in figure 2, where reflection and

transmission spectra for a sample grown on a glass substrate are presented. Here it must be noted that the fact that the reflected and transmitted peaks do not present a flat top is partly due to the presence of disorder, and also to the fact that the samples considered are only 25 layers thick. The extinction length for frequencies close to the stop band edge being larger than that for frequencies closer to the center [14], thin samples are expected to present a rounded shape even in the absence of disorder. We will then use reflection spectra to study the evolution of the Bragg peak associated to diffraction by the (111) family of planes.

In order to carry out a comparison of our experimental results with theory, we have followed two approaches. On one hand we have calculated the photonic band structure associated to our system following the plane wave expansion method (PWEM) [35]. Photonic bands, being an exact solution of the propagation of electromagnetic radiation inside an infinite crystal, cannot account for the optical properties of finite systems. To model the evolution of the experimental spectra as a function of the crystal thickness, we have employed the results provided by the Scalar Wave Approximation (SWA) [36]. In the latter approach, the scalar Maxwell´s equations are solved for the infinite crystal considering the radiation inside the crystal to be the sum of an incident beam, and a beam diffracted by the (111) family of planes. By doing this, an analytic expression for the dispersion relation $\mathbf{k}(\omega)$ inside the crystal for propagation perpendicular to those planes is obtained, which can be used to model transmission and reflection spectra for finite systems using the appropriate boundary conditions [37]. This approach, although basic, has proved to reproduce well the experimental results [22, 13, 32].

Figure 3 shows experimental and calculated results for a sample 23 layers thick grown on glass substrate. On the left panel, bands calculated using the SWA and the

exact PWEM are plotted together. On the right panel, experimental and theoretical reflectivity spectra are shown. The vertical axis represents energy in reduced frequency units a/λ where a is the lattice parameter of the fcc structure and λ the wavelength of light in vacuum. The horizontal axis represents absolute reflectance. Experimental and calculated spectra present a pronounced reflectivity peak which coincides with the position of the stop band which opens in the dispersion relation as a consequence of diffraction by the (111) family of planes. At both sides of this peak, secondary oscillations are found. These oscillations appear in an spectral region were the dispersion relation of the infinite crystal is linear. In this region, the sample may be considered as a homogeneous medium with an effective refractive index, and the secondary oscillations can then be interpreted as Fabry-Perot fringes arising due to reflection at the front and rear facets of the sample [36]. From the spectral separation of the fringes in the low energy region, where the crystal can be approximated by an average effective refractive index, we may extract the crystal thickness. When comparing both spectra, we see how the spectral position of the Bragg peak and the secondary oscillations coincide well, the latter slightly departing from the common behaviour for reduced frequencies larger than 0.85, where experimental ones seem to become closer together. This coincides with the fact that the dispersion relation predicted by the SWA presents steeper slope in the high energy region than that given by the exact PWEM, that predicts a smaller effective refractive index. This difference is probably due to the absence of higher order diffractions, as well as diffraction by families of planes other than the (111), in the SWA calculations. Besides this, it can be seen that the width and height of both peaks disagree. These differences will be addressed later on.

When comparing experimental reflectance spectra with calculated photonic bands, the frequencies located at the FWHM edges of the Bragg peak are usually associated to the edges of the stop band [29, 33] and the center frequency of the peak to the stop band center [38]. We now proceed to study how these parameters, as well as the FWHM itself, vary as the number of lattice planes parallel to the sample surface is increased. In order to discriminate which of these parameters is affected by the substrate we have carried out normal incidence reflectivity measurements for samples grown on silicon wafers and glass microslides. For these measurements a non polarized white light beam from a tungsten lamp 375μm in diameter with an angular aperture of 6º full angle was used. Detection was performed using and indium antimonide detector.

Experimental results and theoretical predictions are presented in figures 4 and 5. ω_+ and ω_- correspond to the high and low frequency edges of the FWHM, expressed in reduced units a/λ. ω_0 corresponds to the FWHM center. Open and closed circles correspond to measured data for samples grown on glass microslides and silicon wafers respectively. Theoretical SWA predictions for finite samples grown on silicon and glass substrates are shown as solid and dashed curves respectively. The horizontal dotted and solid lines correspond to theoretical results for the infinite crystal predicted by the PWE and SWA methods respectively. In figure 4a, the evolution of the edges as the number of lattice planes increases is plotted. For both types of sample substrates we can see a dependence of the experimental edges position with the crystal thickness, although for samples grown on a silicon substrate the edges are shifted to higher frequencies as compared to those grown on glass. It is for samples thicker than 30 layers that both types seem to follow a common trend, approaching the infinite crystal limits predicted by the exact PWEM. This behavior is qualitatively reproduced by the approximated SWA results. The difference between the two types of samples becomes more clear if

we study ω_0 as a function of crystal thickness as in figure 4b. Here we can appreciate how depending on the substrate on which the sample lies, glass or silicon, the peak center will monotonically increase or decrease in frequency with the number of (111) lattice planes before merging into a common behavior for samples thicker than 30 planes, this behavior coinciding with that predicted by the PWE for the infinite system. The SWA also reproduces qualitatively these results for finite crystals, although it can be seen that the SWA peak centers converge towards the infinite crystal limit obtained in that approach. As can be seen in figure 3, this limit is clearly different from that predicted by the exact PWE.

The only difference between the two substrates being its refractive index, the above results indicate that in the formation of the Bragg peak, a feature which ultimately will reveal the stop band and which happens as a consequence of multiple scattering between parallel lattice planes, reflections at the sample interfaces have a crucial importance in determining its spectral position. Therefore, neither the peak center ω_0 nor the FWHM edges, ω_+ and ω_-, offer information about the properties intrinsic to the photonic crystal itself, and will not be considered further. Nevertheless, these results are interesting on its own, and will be the subject of a future work.

Figure 5 presents experimental results and theoretical predictions for the evolution of the FWHM of samples grown on both types of substrate. It can be seen that the results are coincident in both cases, indicating that the FWHM of the Bragg peak is an intrinsic signature of the photonic crystal, and therefore independent of the substrate used. The experimental FWHM of the Bragg peak is seen to decrease monotonically as the number of lattice planes increases [13], until reaching a stationary value practically the same as that predicted by the exact PWEM for samples 35 layers thick. Now again the SWA qualitatively reproduces experimental results, although overestimating them in

a systematic way. A possible reason for this disagreement is to be found comparing the dispersion relation for the infinite crystal calculated by the SWA and PWEM approaches (fig. 3, left panel). We find that the stop band width predicted by the SWA overestimates the exact result of the PWEM, as indicated by the horizontal lines in figure 5.

Beside the limitations of the SWA, an additional source of error could be in the presence of an angular aperture on the probing beam. This would introduce a broadening in the experimental peak which can been estimated to be less than 0.5% for this aperture, and can therefore be neglected.

IV. EFFECTS OF DISORDER

In this section we will examine the effect of disorder on the previous measurements, in order to determine whether it contributes to the observed width or, on the contrary, the latter comes solely from finiteness and photonic interaction.

As mentioned above, in the presence of disorder the optical properties of a photonic crystal are altered with respect to the ideal case. For crystals presenting a mosaic spread the width of the Bragg peak has been observed to present an inhomogeneous broadening [19, 32]. In our case we believe the effect of this type of disorder will be negligible due to the way the samples are grown. Stacking faults along the (111) direction, a defect commonly found in artificial opals, are known not to affect the optical properties of the crystal, at least in the region of low energies where we are interested [16, 17, 20].

In the presence of grain boundaries, point defects, and dislocations, the propagation of light inside a photonic crystal becomes diffuse [14, 19].This affects the optical properties in two different ways depending on the spectral region considered.

While for frequencies outside the stop band light propagation becomes diffuse in a cone around the zero order beam [14, 19], for frequencies contained in the stop-band a combination of an interplay between coherent Bragg scattering and incoherent diffuse scattering, and the effect of energy bands leads to an enhancement of diffuse intensity for those frequencies near the edges of the stop band [19, 39]. The bandstructure of our system being similar to that of refs. 19 and 39, we expect a similar behavior. If we consider the photonic bands for directions close to the ΓL direction, i.e: normal incidence (see figure 6), we can see how those frequencies contained in the stop band for normal incidence are associated with a cone of forbidden directions, the angle of which increases as the frequency approaches ω_+. This is schematically shown in figure 6 for two frequencies located near ω_+ and ω_- respectively.

We have estimated the diffuse intensity in our measurements in a way analogous to that in ref. 19, as the difference between the incident intensity and the sum of the reflected and transmitted ones in the direction of normal incidence, assuming a negligible absorption for polystyrene in the spectral range under consideration [40]. Results for samples grown on glass, having different thicknesses are presented in figure 7. We can appreciate a diffuse background that increases with frequency and sample thickness. In the spectral region where the Bragg peak appears, we observe the above mentioned maxima coinciding with the band edges, and minimum for intermediate frequencies. Here it must be noted that the diffuse intensity peaks provide a good assessment of the band edges as estimated from reflectance spectra.

In order to determine the effect that this incoherent scattering could have on the measurements presented in figures 5, we have compared the FWHM of samples which, having the same number of layers presented a lower reflectivity, indicating a larger effect of disorder. To carry out these measurements we employed samples grown at

temperatures between 55ºc and 40ºc. The results are shown on figure 8. Here we can see that for variations in reflected intensity above 15%, no noticeable changes in the FWHM are observed, or in ω_0 for that matter. Thus we believe that, although the existence of a stronger diffuse scattering for those frequencies near the stop band edges may affect the FWHM of the reflectivity peak, it is probably not significant in our case, and we can consider the observed width as a combination of finite size effects and photonic interaction of the system.

From the transmission spectra for samples grown at 45ºC having different thickness we have estimated the attenuation length ℓ_B at midgap. This is usually defined as $\ell_B = \frac{LnT}{L}$, where T is the transmittance and *L* the crystal thickness. In figure 9 we have plotted *LnT* versus the crystal thickness for the experimental results and the SWA predictions. Both results present an excellent agreement for thickness up to 10 layers, where a linear dependence has not yet been achieved. For thicker crystals a linear trend can be observed in both cases, although a different slope is to be found. We have estimated the extinction length for the experimental results to be 8±0.5 layers, larger than the 5 layers predicted by the SWA. This coincides with previous comparisons of disordered media with ideal systems [14].

V. ANGLE RESOLVED REFLECTIVITY

Having determined the threshold thickness for infinite crystal behavior we proceed to study the angular dependence of the Brag peak. For the angle resolved specular measurements a non polarized white light beam from a tungsten lamp 1mm in diameter was used with an angular aperture of 3º full angle. The angular range covered in the experiments was limited from θ=20º to θ=75º due to limitations imposed by the experimental set-up, where θ is the angle between the incident beam and the normal to

the crystal surface. As the angle of incidence increases, the size of the spot increases to a maximum value of ~2.5mm. Prior to carrying out reflectivity measurements as a function of angle, the samples were studied under normal incidence, and the regions to be probed were chosen so that the reflectivity spectrum remained constant over regions ~3mm^2 in dimension. The criteria followed were that the absolute reflectance of the Bragg peak did not change more than 10%, and the position of the Fabry-Perot oscillations remained at a fixed position, the latter indicating a constant sample thickness over the probed area.

In angle resolved specular measurements, the experiment is such that the incident and diffracted wave vectors, as well as the normal to the sample surface are contained in a plane perpendicular to the rotation axis and the sample surface (see Fig. 10). When carrying out these measurements, the sample was oriented with respect to this diffraction plane by using the observed diffraction pattern. According to the above discussion if the microslide is rotated around its vertical axis, parallel to the sample growth direction, the diffraction plane will coincide with a plane passing through the Γ, L and U (K) points in the Brillouin zone [41] (see Fig. 10a). If, on the other hand, the sample is placed such that the rotation axis is now perpendicular to the growth direction but parallel to the sample surface, it is the plane spanned by the Γ, L and W points that we must consider (see Fig. 10b).

In figure 11 reflectivity spectra for different angles of incidence are plotted for two equivalent orientations of a sample 34 layers thick. In figure 11a, the growth direction is parallel to the rotation axis, as in figure 10a. In figure 11b, the sample has been rotated 60º around its surface normal. According to the above discussion in both cases the parallel component of the incident wavevector points along the LU or LK

segment in the hexagonal facet of the Brillouin zone. Therefore the bands used for comparison were calculated along those directions as shown in figure 11c.

We see how for small angles of incidence the experimental reflectivity peak follows the calculated lowest energy bands, which quantitatively follow Bragg´s law for the (111) family of planes. As the angle of incidence increases we observe how a new reflectance peak appears for reduced frequencies above those of the Bragg peak. For even larger angles the Bragg peak disappears and it is only the high frequency peak that remains. This effect has been observed for titania inverse opals in ref. 33, and for direct opals in ref. 38. It has been associated with a wave coupling phenomenon taking place when the incident wavevector reaches the U point, and diffraction by the (111) and (200) families of planes are excited simultaneously causing reflectance spectra to deviate from simple Bragg diffraction [33]. In our case this avoided crossing, which may be caused by simultaneous diffraction by the (111) and (200) (i.e: U point) or the (111) and (11-1) (i.e: the K point), taken as the closest point between the two peaks, takes place for a reduced frequency of ~0.74 and a $\mathbf{k}_{//}$ ~0.6, which coincides with the theoretical predictions.

Figure 12 shows identical measurements when the sample is oriented such that the parallel component of the incident wavevector points along the LW direction in the Brillouin zone. By reasoning as before, this is achieved when the sample rotates around an axis which is contained in the sample surface but either perpendicular (see figure 10b) or at 30º with respect to the growth direction. Figures 12a and 12b represent the two cases. Here the situation is more complex than before, since as the incident wavevector points along the ΓW direction, its parallel component lying in the LW segment, the Bragg condition is simultaneously satisfied for three families of planes,

that is the (111), (200) and (11-1). The bands that account for the data here were calculated along the LW direction and are plotted in figure 12c.

Now we see that, as predicted by the calculated bands, the Bragg peak follows Bragg´s law for a larger angular range and it is not until reaching 55º that a second peak appears at higher frequency. This is to be expected since the W point is the point lying furthest from the origin of the Brillouin zone, at the Γ point, and furthest from L in the hexagonal facet. At 60º we see how the Bragg peak branches, a new reflectivity peak appearing at lower frequencies, while the high frequency peak observed for 54º becomes more intense and moves to a lower frequency, as predicted by the calculated bands. For larger angles, the low frequency peak decreases in intensity and frequency, while the high frequency peak that appeared at 54º merges with the Bragg peak, which presents a complicated shape with two shoulders. Although the fact that Bragg peak is present at all angles has not a plausible explanation at this time, the overall behavior of reflectivity peaks is well accounted for by the exact PWE calculation.

VI. CONCLUSIONS

In conclusion, we have performed a study of the optical properties of opal based photonic crystals by means of reflectivity and transmission measurements. Using non destructive structural characterization of the samples involving only optical techniques we have determined the thickness and orientation of our samples.

This has allowed us to characterize the finite size effects present in the optical properties of our samples. In doing so we have been able to discriminate those features present in experimental spectra which depend on the substrate on which the sample is grown, from those intrinsic to the interaction of the crystal with electromagnetic radiation. A threshold thickness has been found for this refractive index modulation, for

which the optical properties of the crystal are independent of the substrate. For crystals having a larger refractive index contrast, although finite size effects should disappear for fewer layers, this qualitative behavior should prevail. Nevertheless, a similar study for crystals possessing a PBG would be interesting not only for the spectral region studied here, but also in the high energy region where the PBG should manifest. These results will be relevant in further photonic crystal characterization. Finally, a study of the photonic bands in the surroundings of the L point in the Brillouin zone has been performed by means of angle resolved reflectivity.

ACKNOWLEDGEMENTS

The authors would like to thank Prof. J. Sánchez-Dehesa for fruitful discussions.

[1] E. Yablonovitch, Phys. Rev. Lett. **58**, 2085 (1987)

[2] S. John, Phys. Rev. Lett. **58**, 2486 (1987)

[3] H.S. Sözüer, J. W. Haus, and R. Inguva, Phys. Rev. B **45**, 13962 (1992)

[4] K. Busch, and S. John, Phys. Rev. E **58**, 3896 (1998)

[5] S. John and J. Wang, Phys. Rev. Lett., **64**, 2418 (1990)

[6] E. Paspalakis, N. J. Kylstra, and P. L. Knight, Phys. Rev. A **60**, R33 (1999)

[7] H. Kosaka, T. Kawashima, A. Tomita, N. Notomi, T. Tamamura, T. Sato and S. Kawakami, Phys. Rev. B **58**, 10096 (1998)

[8] M. Notomi, Phys. Rev. B **62**, 10696 (2000)

[9] O. Painter, R. K. Lee, A. Scherer, A. Yariv, J. D. O´Brien, P. D. Dapkus, and I. Kim, Science **284**, 1819 (1999)

[10] H. Kosaka, T. Kawashima, A. Tomita, N. Notomi, T. Tamamura, T. Sato, and S. Kawakami, Appl. Phys. Lett. **74**, 1212 (1999)

[11] A. Chutinan, S. John, and O. Toader, Phys. Rev. Lett. **90**, 123901 (2003)

[12] K. Busch, C. R. Physique **3**, 53 (2002)

[13] J. F. Bertone, P. Jiang, K. S. Hwang, D. M. Mittleman, and V. L. Colvin, Phys. Rev. Lett. **83**, 300 (1999)

[14] Y. A. Vlasov, M. A. Kaliteevski, and V. V. Nikolaev, Phys. Rev. B **60**, 1555 (1999)

[15] A. F. Koenderink, M. Megens, G. van Soest, W. L. Vos, and A. Lagendijk, Phys. Lett. A **268**, 104 (2000)

[16] Y. A. Vlasov, V. N. Astratov, A. V. Baryshev, A. A. Kaplyanskii, O. Z. Karimov, and M. F. Limonov, Phys. Rev. E **61**, 5784 (2000)

[17] V. Yannopapas, N. Stefanou, and A. Modinos, Phys. Rev. Lett. **86**, 4811 (2001)

[18] J. F. Galisteo-López and W. L. Vos, Phys. Rev. E **66**, 36616 (2002)

[19] V. N. Astratov, A. M. Adawi, S. Fricker, M. S. Skolnick, D. M. Whittaker, and P. N. Pusey, Phys. Rev. B **66**, 165215 (2002)

[20] Z. L. Wang, C. T. Chan, W. Y. Zhang, Z. Chen, N. B. Ming, and P. Sheng, Phys. Rev. E **67**, 16612 (2003)

[21] D. Felbacq and R. Smaâli, Phys. Rev. B **67**, 85105 (2003)

[22] P. Jiang, J. F. Bertone, K. S. Hwang, and V. L. Colvin, Chem. Mater. **11**, 2132 (1999)

[23] J. W. Goodwin, J. Hearn, C. C. Ho, and R. H. Ottewill, Colloid and Polimer Sci. **252**, 464 (1974)

[24] V. N. Astratov, V. N. Bogomolov, A. A. Kaplyanskii, A. V. Prokofiev, L. A. Samoilovich, S. M. Samoilovich, and Y. A. Vlasov, Nuovo Cimento **17**, 1349 (1995)

[25] R. Mayoral, J. Requena, S. J. Moya, C. López, A. Cintas, H. Migues, F. Meseguer, L. Vázquez, M. Holgado, and A. Blanco, Adv. Mater. **13**, 409 (1997)

[26] W. L. Vos, R. Sprik, A. van Blaaderen, A. Imhof, A. Lagendijk, and G. H. Wegdam, Phys. Rev. B **53** 16231 (1997)

[27] M. Holgado, F. García-Santamaría, A. Blanco, M. Ibisate, A. Cintas, H. Míguez, C.J. Serna, C. Molpeceres, J. Requena, A. Mifsud, F. Meseguer and C. López, Langmuir **15**, 4701 (1999)

[28] H. Migues, C. López, F. Meseguer, A. Blanco, L. Vázquez, R. Mayoral, M. Ocaña, V. Fornés, and A. Mifsud, Appl. Phys. Lett. **71**, 1148 (1997)

[29] M. S. Thijssen, R. Sprik, J. E. G. J. Wijnhoven, M. Megens, T. Narayanan, A. Lagendijk, W. L. Vos, Phys. Rev. Lett. **83**, 2730 (1999)

[30] M. Tomita, K. Tacano, and T. G. M. Van de Ven, J. Colloid Interface Sci. **92**, 367 (1983)

[31] T. Yamasaki and T. Tsutsui, Jpn. J. Appl. Phys., **38**, 5916 (1999)

[32] Y. A. Vlasov, M. Deutsch, and D. J. Norris, Appl. Phys. Lett. **76**, 1627 (2000)

[33] H. M. Van Driel and W. L. Vos, Phys. Rev. B **62**, 9872 (2000)

[34] J. F. Galisteo-López, F. López-Tejeira, S. Rubio, J. Sánchez-Dehesa, and C. López, Appl. Phys. Lett. (in press)

[35] Photonic band structures are computed using a plane wave basis in an iterative implementation as described in S. G. Johnson and J. D. Joannopoulos, Opt. Express **8**, 173 (2001)

[36] K.W. Shung and Y. C. Tsai, Phys. Rev. B **48**, 11265 (1993)

[37] When using the SWA, the Maxwell-Garnett effective dielectric constant was substituted for the zero order term in the expansion of the dielectric constant, which has been shown to better reproduce the exact PWE results in the long wavelength limit in; S. Datta, C. T. Chan, K. M. Ho, and C. M. Soukoulis, Phys. Rev. B **48**, 14936 (1993)

[38] S. G. Romanov, T. Maka, C. M. Sotomayor Torres, M. Muller, R. Zentel, D. Cassagne, J. Manzanares-Martinez, and C. Jouanin, Phys. Rev. E **63**, 56603 (2002)

[39] M. A. Kaliteevski, J. Manzanares Martinez, D. Cassagne, and J. P. Albert, Phys. Rev. B **66**, 113101 (2002

[40] T. Inagaki, E. T. Arakawa, R. N. Hamm, and M. W. Williams, Phys. Rev. B **15**, 3243 (1977)

[41] For opal based photonic crystals, although the U and K points are not identical, the energy bands for the LU and LK directions in the Brillouin zone coincide, and they will be considered as one in what follows.

Figure captions:

FIG. 1. (a) Scanning electron micrograph of the sample surface showing the hexagonal order present. The arrow indicates the growth direction. Inset corresponds to the Fourier transform of the micrograph. (b) Point defects and dislocations present in the sample. (c) Crack separating two domains having the same orientation. (d) Side view of a 7 layers thick sample.

FIG. 2. Normal incidence reflectance and transmittance spectra for a sample 25 layers thick grown on a glass substrate.

FIG. 3. (a) Dispersion relation for the infinite system calculated using the PWE (SWA) method is presented as solid (dashed) lines. (b) Experimental and calculated normal incidence reflectivity spectra for a sample 23 layers thick are shown as thick and thin solid lines respectively.

FIG. 4. (a) Experimental edges, ω_+ and ω_-, of the FWHM reflectivity peaks for samples width a different thickness are plotted as open (solid) circles for samples grown on glass (silicon) substrate. SWA predictions for the finite system appear as dashed (solid) curves for the glass (silicon) cases. Horizontal solid (dotted) lines correspond to the SWA (PWE) predictions for the infinite system. (b) Experimental and theoretical results for the center ω_0 of reflectivity peaks as a function of sample thickness. Symbols are the same as those on (a).

FIG. 5. FWHM of reflectivity peaks for samples grown on silicon and glass substrates, as a function of the sample thickness. Theoretical and experimental data are presented with same symbols as those on figure 4.

FIG. 6. a) Bandstructure calculated along the ΓLU,K,W direction. The horizontal dashed lines indicate two frequencies near the high (ω_+) and low (ω_-) energy edges of the pseudogap. b) Brillouin zone of the fcc lattice. Range of forbidden directions for the above frequencies indicated in the surroundings of the hexagonal facet, pertinent to our measurements.

FIG. 7. Diffuse intensity spectra estimated for samples with different thickness. From top to bottom: 45, 35, 25, 15 and 10 layers.

FIG. 8. FWHM for samples having the same thickness but presenting a different reflectivity. Groups of symbols with increasing a/λ correspond to samples with 10, 17, 22 and 39 layers.

FIG. 9. Logarithm of the transmittance at the center frequency of the Bragg peak as a function of the number of layers. Experimental results appear as circles, and SWA predictions as a solid line. Inset shows the same results in a linear scale.

FIG. 10. The sample (S) is denoted by the dark gray region of the microslide (M). The incident (**K**in) and diffracted (**K**out) wave vectors as well as the normal to the sample surface (N) are contained in the diffraction plane. The growth direction is indicated by an arrow. (a) If the sample is rotated about an axis parallel to the growth direction, we

must consider the plane passing through the Γ, L and U points in the Brillouin zone. (b) When the rotation axis is perpendicular to the growth direction, it is the plane spanned by the Γ, L and W points that we must consider.

FIG. 11. (a) Reflectivity spectra for different angles of incidence as the sample is rotated around an axis parallel to its growth direction. (b) Reflectivity spectra when the rotation axis is rotated 60º with respect to the growth direction in the surface plane. (c) Calculated bands (lines) along the LU direction, and experimental reflectivity peaks (solid and open circles) for the (a) and (b) situations. The dashed line indicate the boundary of the first Brillouin zone at the U (or K) point.

FIG. 12. (a) Reflectivity spectra for different angles of incidence as the sample is rotated around an axis perpendicular to its growth direction. (b) Reflectivity spectra when the rotation axis is rotated 30º with respect to the growth direction in the surface plane. (c) Calculated bands (lines) along the LW direction, and experimental reflectivity peaks (solid and open circles) for the (a) and (b) situations. The dashed line indicate the boundary of the first Brillouin zone at the W point.

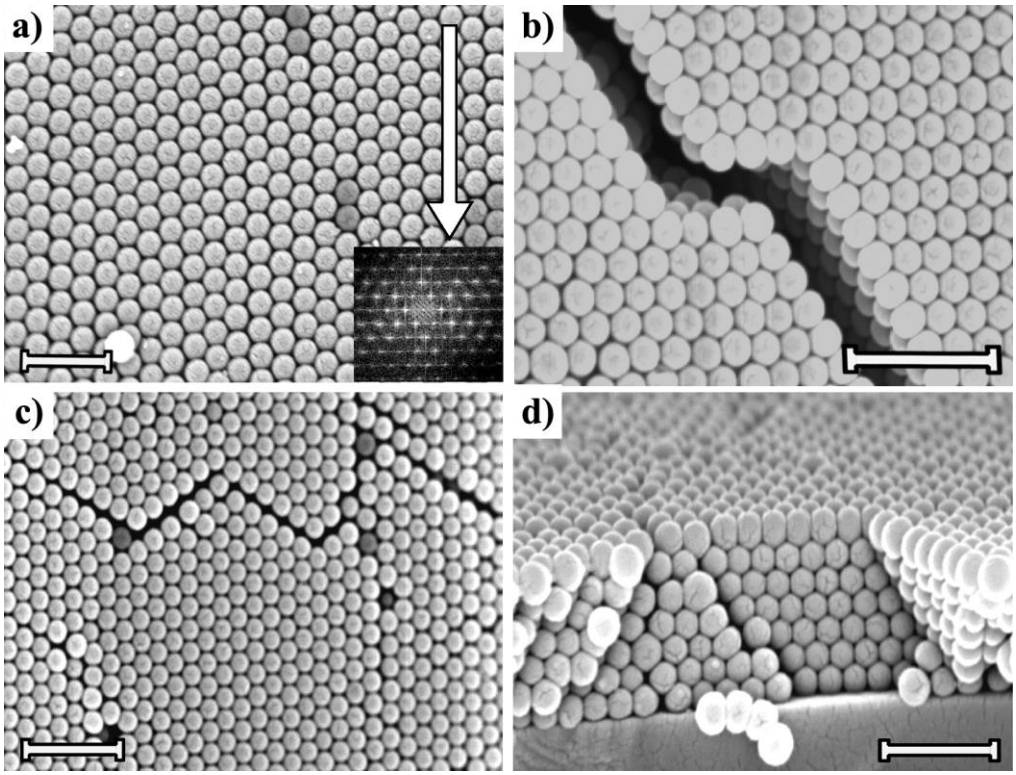

J.F. Galisteo-López *et al.* Figure 1

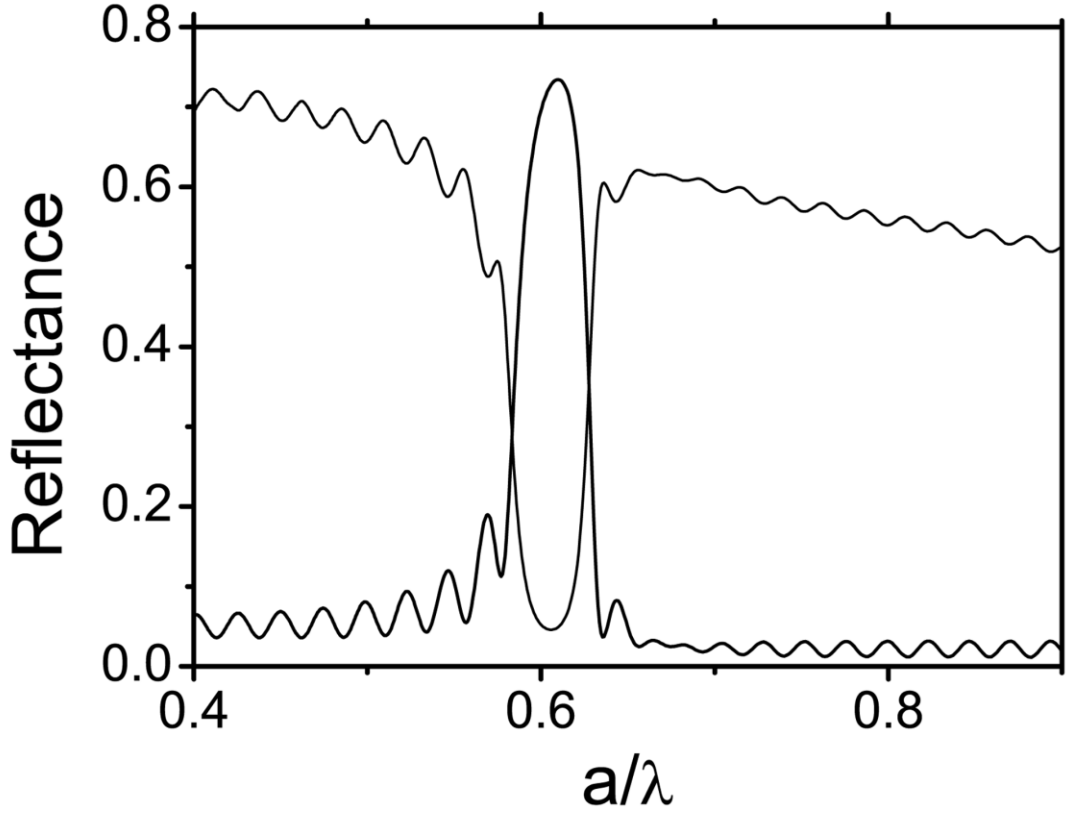

J.F. Galisteo-López *et al.* Figure 2

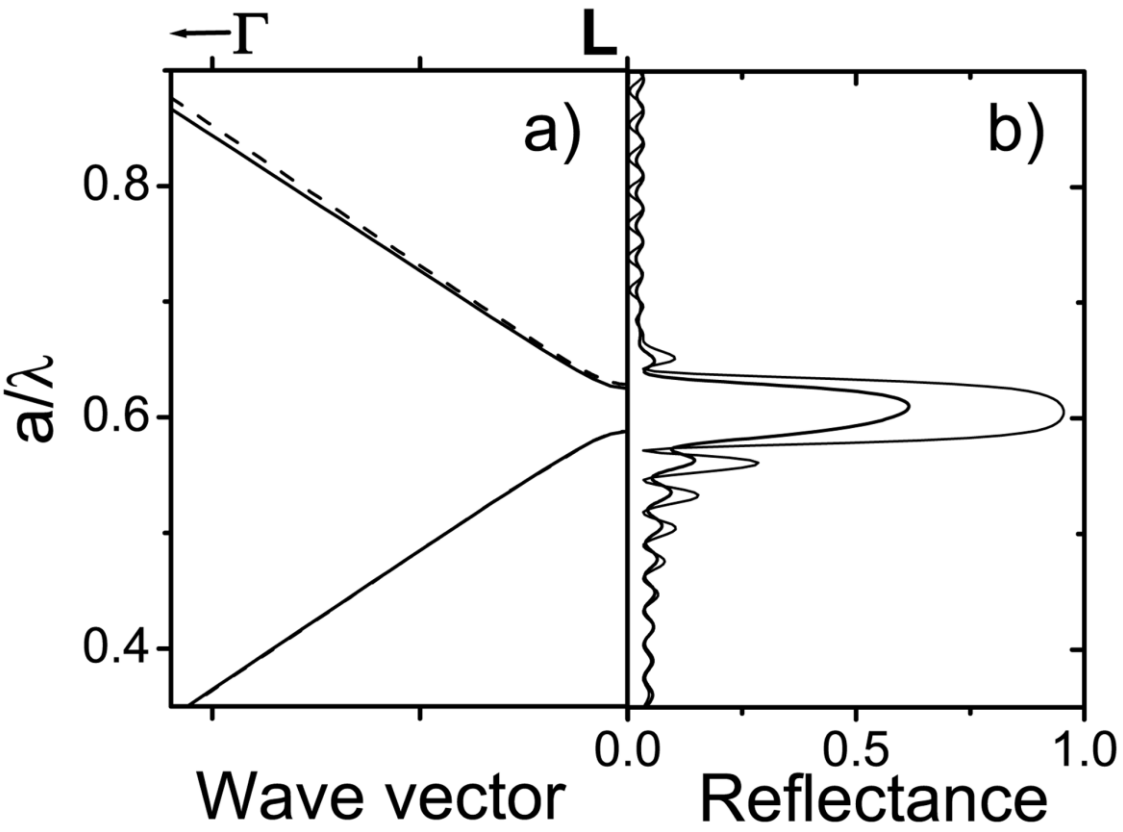

J.F. Galisteo-López *et al.* Figure 3

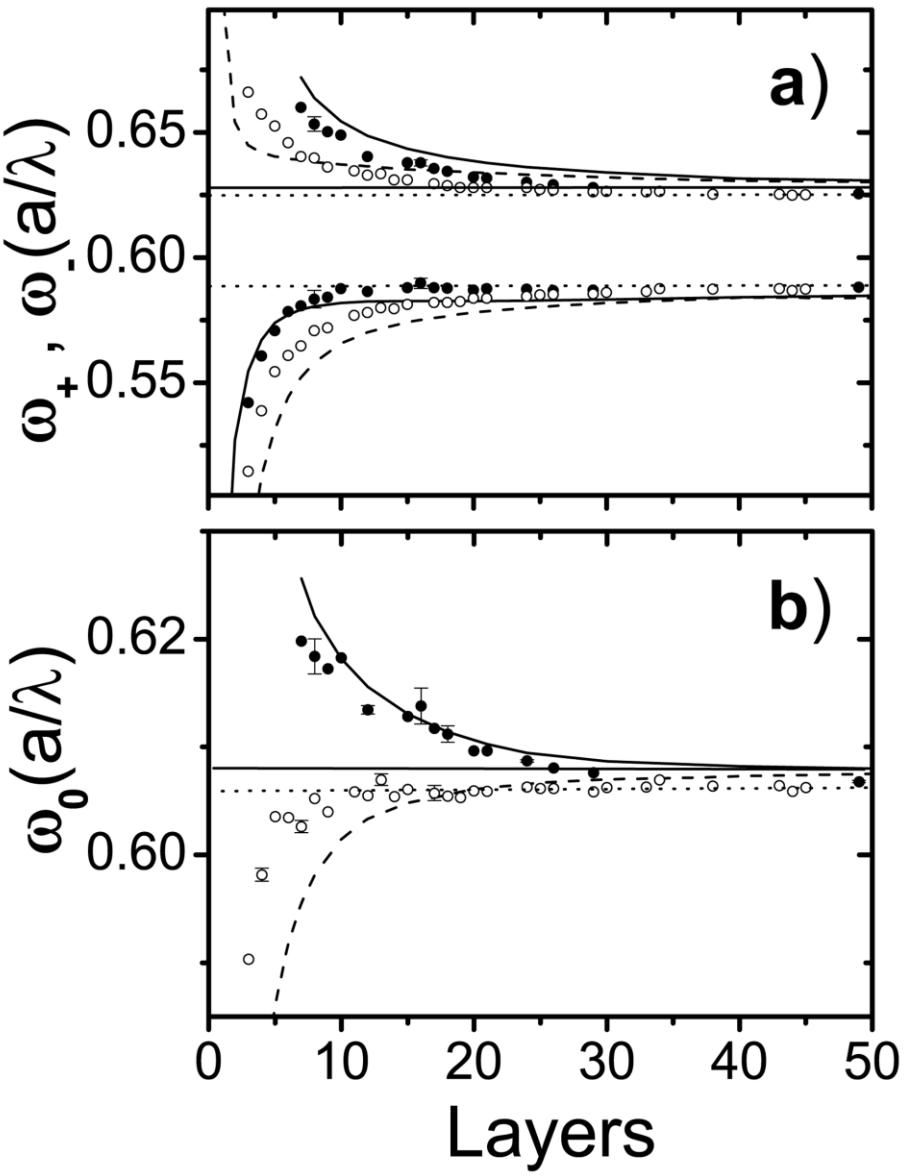

J.F. Galisteo-López *et al.* Figure 4

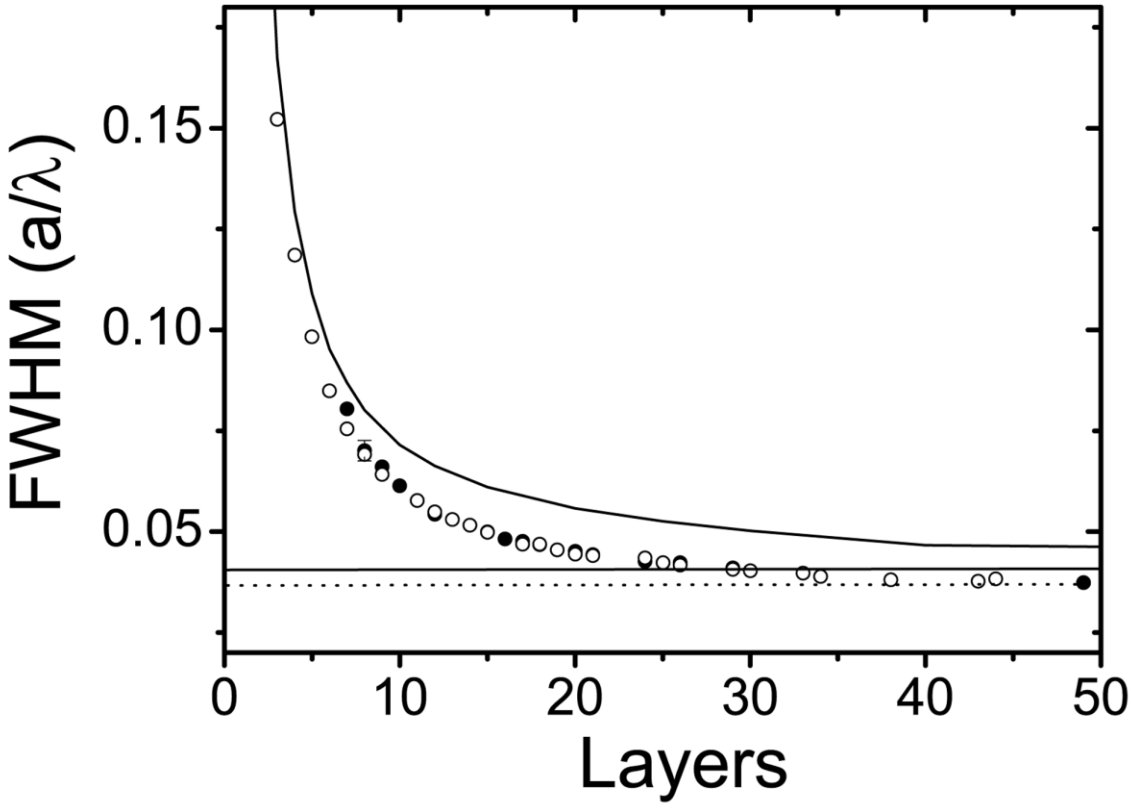

J.F. Galisteo-López *et al.* Figure 5

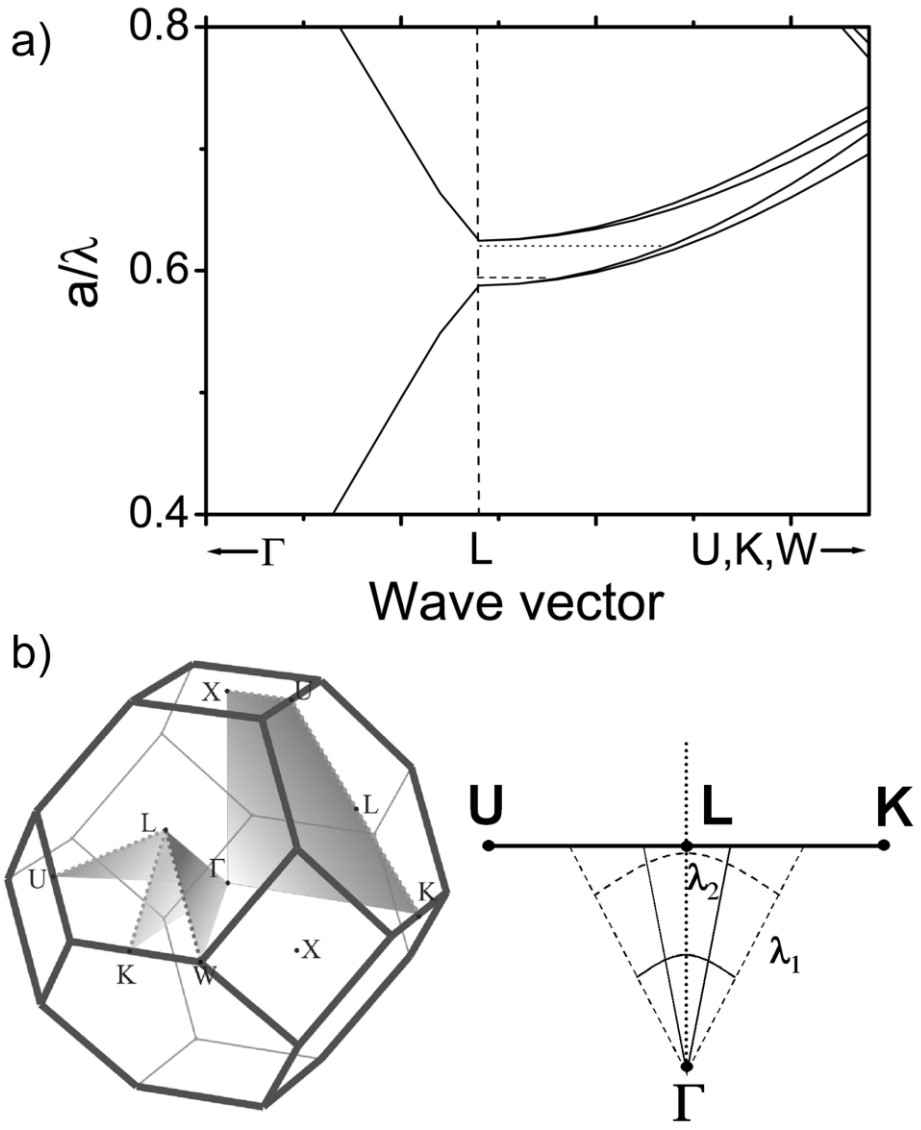

J.F. Galisteo-López *et al.* Figure 6

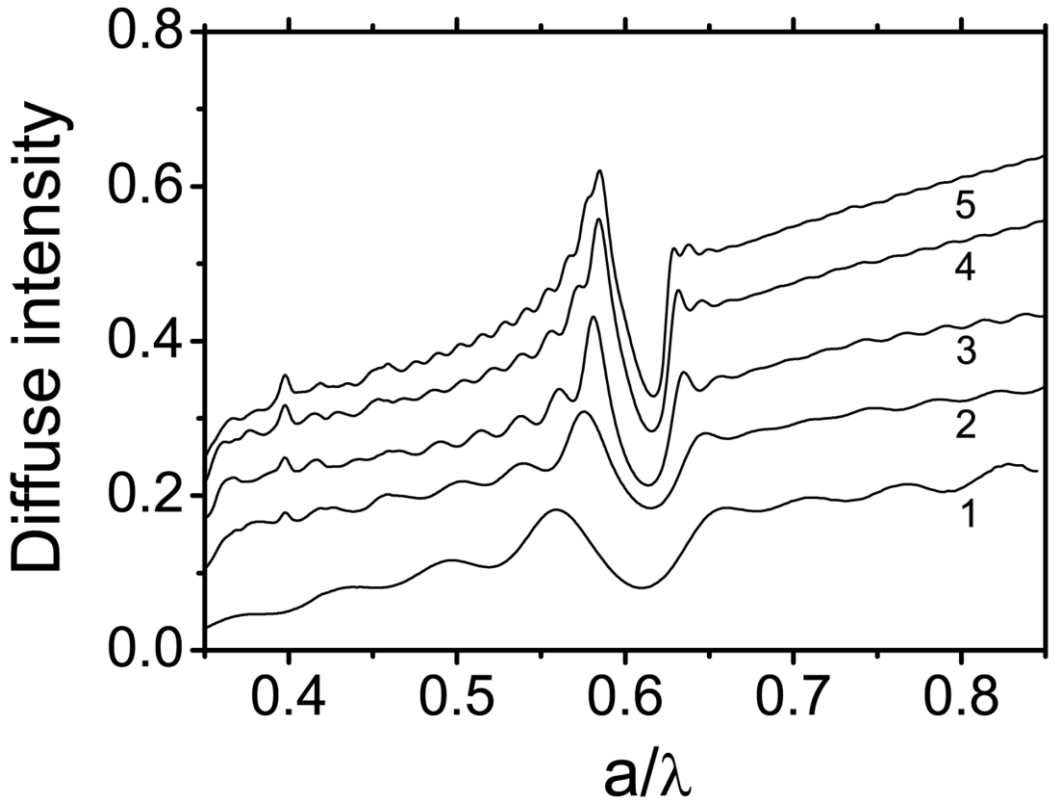

J.F. Galisteo-López *et al.* Figure 7

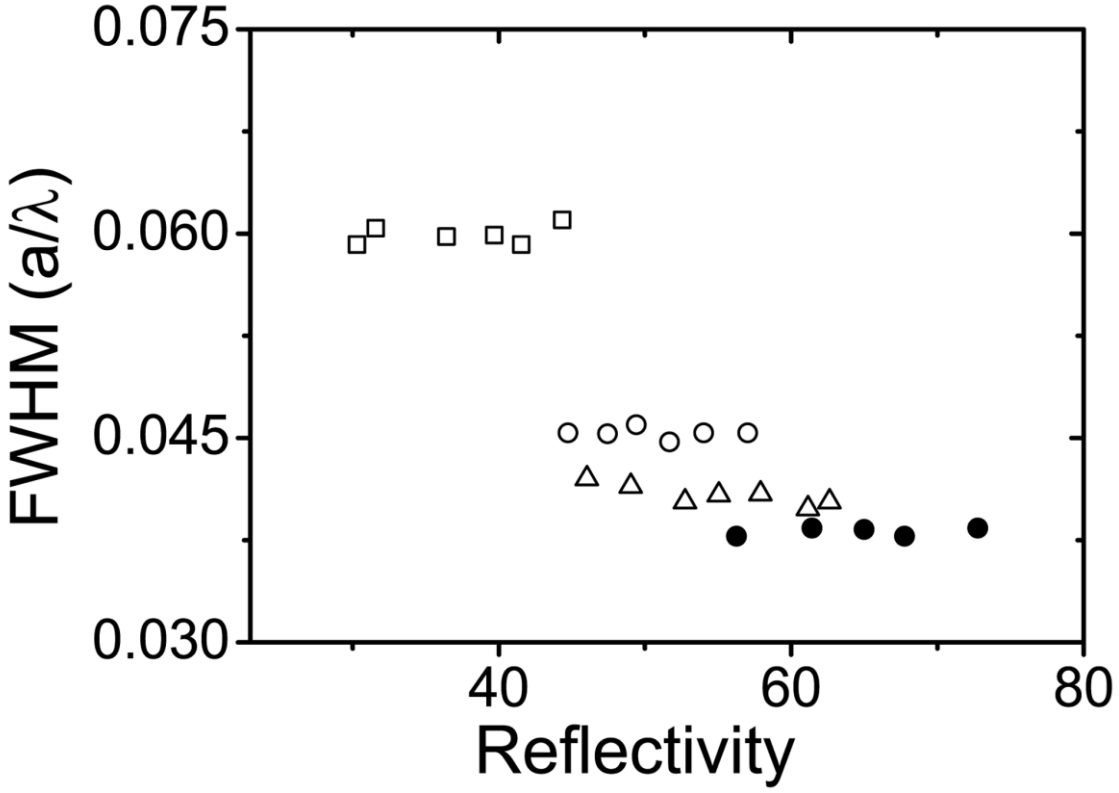

J.F. Galisteo-López *et al.* Figure 8

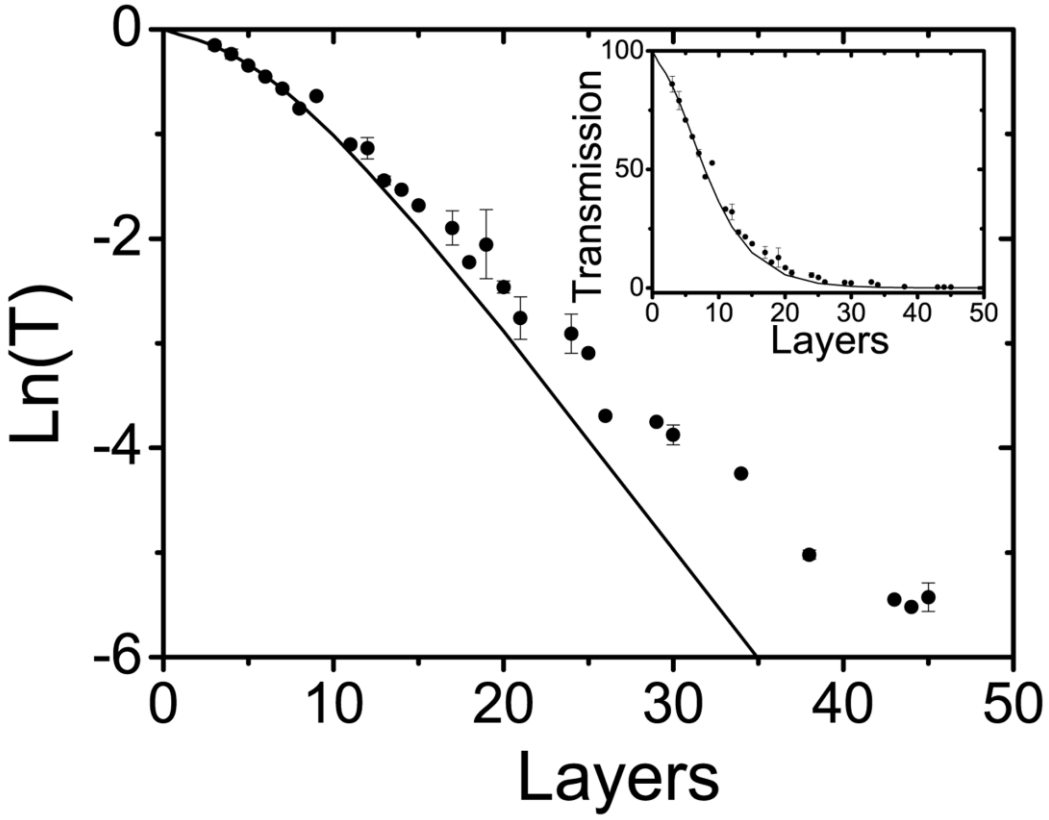

J.F. Galisteo-López *et al.* Figure 9

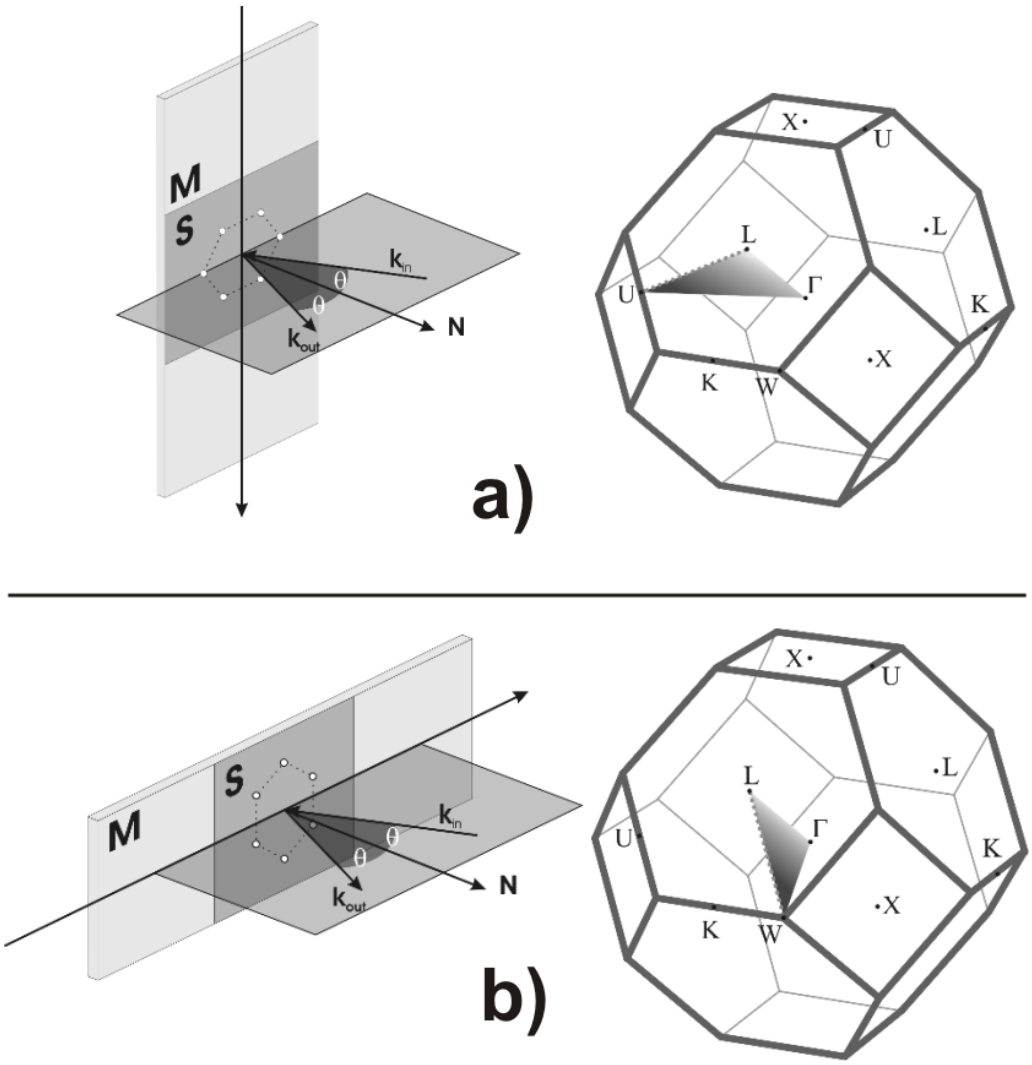

J.F. Galisteo-López *et al.* Figure 10

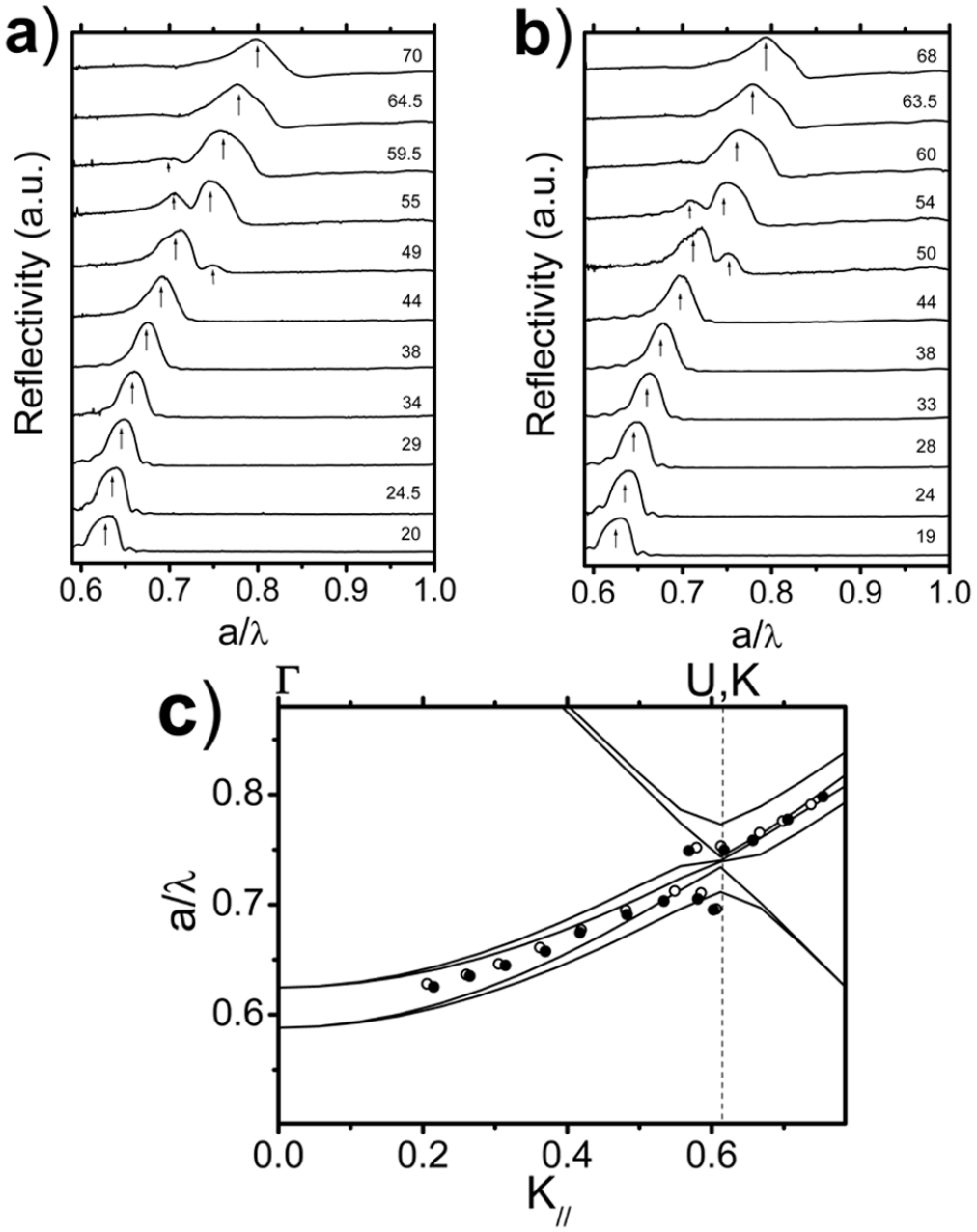

J.F. Galisteo-López *et al.* Figure 11

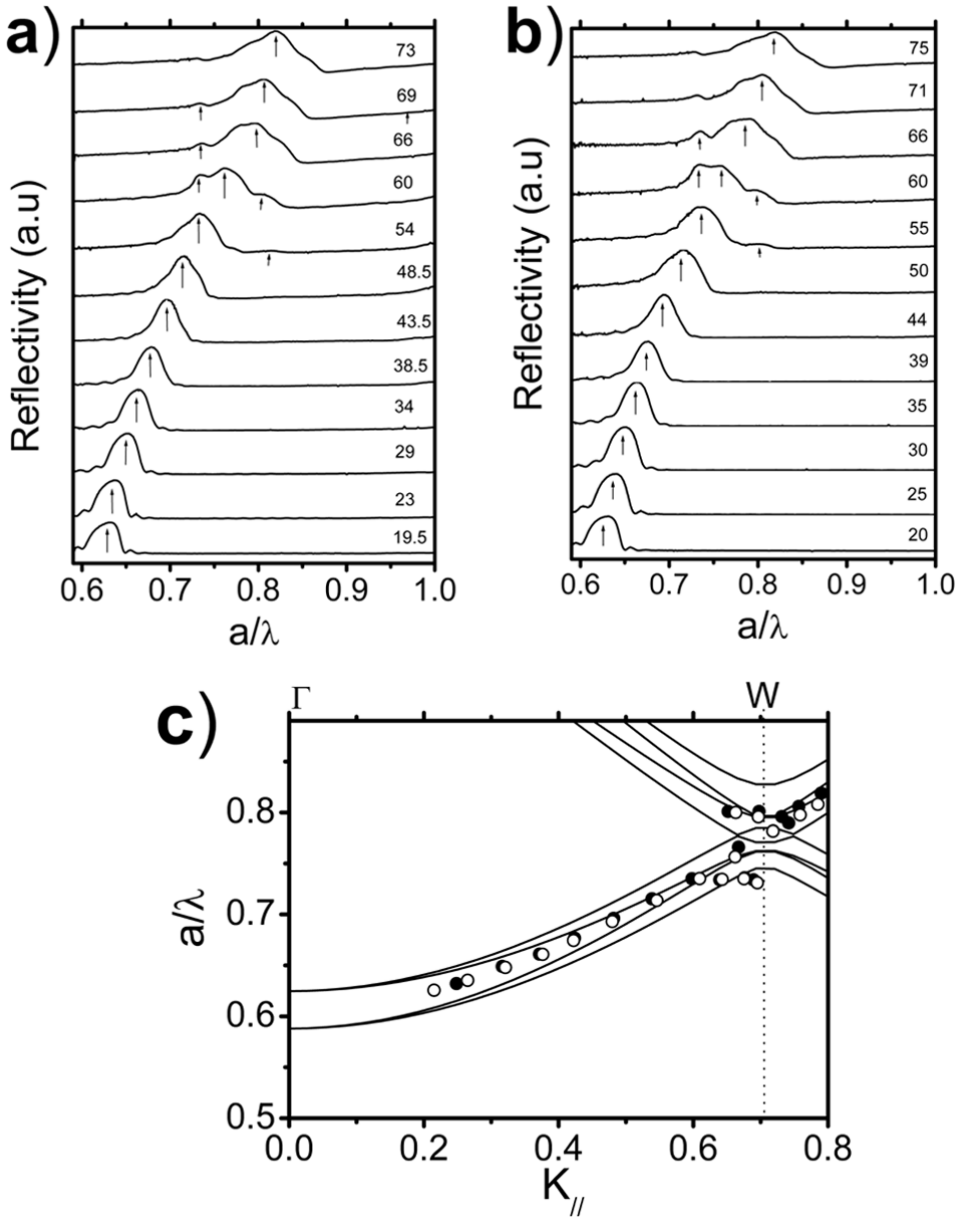

J.F. Galisteo-López *et al.* Figure 12